Journal of Materials Chemistry A

ROYAL SOCIETY OF CHEMISTRY

PAPER

View Article Online
View Journal

Open Access Article. Published on 09 October 2025. Downloaded on 10/29/2025 11:21:30 PM.
This article is licensed under a Creative Commons Attribution-NonCommercial 3.0 Unported Licence.

Check for updates

Cite this: DOI: 10.1039/d5ta04860e

Ab initio investigations of zwitterionic polymers and their interactions with water and ice

Sara A. Tolba, †[ab] Tamalika Ash †[c] and Wenjie Xia *[c]

Preventing ice formation and accumulation on solid surfaces remains a great challenge across a wide range of applications. The application of anti-icing coatings has emerged as an effective strategy to reduce both ice formation and adhesion. Among those, zwitterionic polymeric coatings have recently demonstrated promising anti-icing performance; however, their interactions with water and ice at a fundamental level are not yet fully understood. In this work, we present an attempt to address this knowledge gap by employing density functional theory (DFT) calculations to present a comprehensive understanding of water-zwitterionic polymer interaction at the atomic and electronic levels. We further explored ice interactions and adhesion with the studied polymers using different sizes of ice clusters and the ice surface. Our study reveals distinct hydration behaviors across the studied four representative zwitterionic polymers – poly(sulfobetaine methacrylate) (polySB), its structural isomer (polySBi), poly(2-methacryloyloxyethyl phosphorylcholine) (polyMPC), and poly(carboxybetaine acrylamide) (polyCBAA) which unveil the molecular origin of their anti-icing performance. Our calculations show that polyMPC forms strong hydrogen bonds with water molecules, while polyCBAA develops a thicker hydration layer. Both polySB and polyMPC significantly deform ice clusters and promote surface lubrication, making ice formation energetically unfavorable within their hydration layers. PolyCBAA shows moderate binding with ice clusters, but substantially deforms the ice surface, promoting a lubricating water-like interfacial layer. In contrast, polySBi exhibits the lowest water adsorption and the weakest anti-icing performance. These molecular-level insights highlight the critical role of charged group arrangements in polymer–water–ice interactions, paving the way for the design of next-generation anti-icing materials.

Received 16th June 2025
Accepted 8th October 2025

DOI: 10.1039/d5ta04860e

rsc.li/materials-a

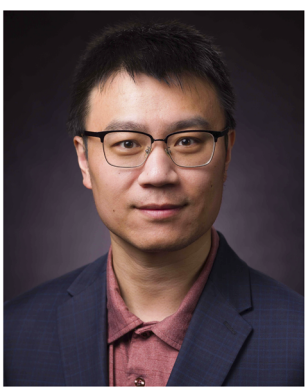

Wenjie Xia

Wenjie Xia is an Associate Professor in the Department of Aerospace Engineering at Iowa State University. He received his PhD from Northwestern University in 2016. His research focuses on the multiscale modeling and computational design of polymers and soft matter to understand and predict the complex behaviors of multifunctional and structural materials. He is a recipient of several prestigious awards, including the NSF CAREER Award, ACS PMSE Young Investigator Award, and ASME Rising Star of Mechanical Engineering.

Introduction

Ice accumulation on surfaces in various engineering applications, such as aircraft, ships, wind turbines, power lines, dams, and renewable energy systems, poses significant challenges, including economic losses and risks of severe accidents.[1–5] Anti-icing coatings play a vital role in advancing energy efficiency and sustainable infrastructure. By preventing ice accumulation, they extend the operational lifespan of infrastructure, reduce reliance on chemical deicing agents, and minimize energy losses associated with deicing processes. These coatings enhance the performance of the infrastructures by lowering maintenance demands and energy consumption. Traditional deicing methods, such as application of salt, glycol-based fluids,[6] silicone grease,[7,8] require frequent reapplication and pose cost and environmental concerns. Passive anti-icing or icephobic surfaces, with low water wettability offer considerable economic, energy, and safety benefits but remain challenging to

[a]Materials and Nanotechnology, North Dakota State University, Fargo, ND, 58108, USA

[b]Center for Computationally Assisted Science and Technology, North Dakota State University, Fargo, ND, 58108, USA

[c]Department of Aerospace Engineering, Iowa State University, Ames, IA, 50011, USA. E-mail: wxia@iastate.edu

† Contributed equally.

Open Access Article. Published on 09 October 2025. Downloaded on 10/29/2025 11:21:30 PM.
This article is licensed under a Creative Commons Attribution-NonCommercial 3.0 Unported Licence.

design due to the complex nature of icephobicity.[9,10] Superhydrophobic surfaces with micro- or nanoscale roughness help limit ice formation and spread, but their texture can reduce effectiveness or durability in certain environments.[11,12] Recent decades have witnessed that coatings with surface charges,[13,14] wetting properties,[15,16] and ions[17] show improved performances in inhibiting and delaying the ice nucleation on the surface.

In this context, zwitterionic polymers have gained attention for anti-icing and low ice adhesion applications due to their strong hydrogen bonding with water, eco-friendly nature, and reduced maintenance requirements offering potential cost and energy savings. Tao *et al.* prepared zwitterionic coating with sulfobetaine methacrylate (SBMA) and oligoethylene glycol dimethacrylate (OEGDMA) *via* UV curing, that can delay freezing up to 126.3 ± 4.0 seconds at −18 °C, compared to ∼3 seconds for bare aluminum.[18] Liang *et al.* synthesized poly-SBMA brushes with ∼60 kPa ice adhesion, a ∼75% reduction in ice adhesion compared to uncoated silicon wafers.[19] Bai *et al.* reported that amphiphilic coatings with polySBMA moieties exhibited excellent antifogging performance due to enhanced polymer–water interactions.[20] Wang *et al.* further improved antibiofouling capabilities of photobioreactors by copolymerizing SBMA and hydrophobic 2, 2, 2-trifluoroethyl methacrylate (TFMA) for microalgae cultivation.[21] The zwitterionic monomer 2-methacryloyloxyethyl phosphorylcholine (MPC), first synthesized by Ishihara and colleagues, displayed excellent antifouling properties, initially limited to protein resistance in single-protein solutions.[22] Its effectiveness stems from structural similarity to polar phospholipid groups, enabling bilayer-like membrane structures that resist protein and cell adhesion.[23] Feng *et al.* successfully grafted MPC onto silicon wafer surfaces by combining self-assembling monolayers with atom transfer radical polymerization (ATRP).[24] Shao and Jiang showed that carboxybetaine (CB) based zwitterionic polymers exhibit superior antifouling properties compared to SB variants.[25] Zhang *et al.* developed a hybrid ionic-covalent cross-linked poly(2-carboxy-*N*, *N*-dimethyl-*N*-(3′-acrylamidopropyl)) (polyCBAA)/sulfonic acid (SA)-Ca^{2+} DN hydrogel that effectively resists nonspecific protein, bacterial, cell, and algal adhesion.[26] Hua *et al.* further synthesized spherical pH-responsive polyCBAA brushes with tunable protein adsorption, demonstrating excellent antifouling performance across varying pH and ionic strengths.[27] Schönemann *et al.* synthesized novel polySBMAs, which structurally differ from the conventional polySBMA by having zwitterionic moieties oriented differently with respect to the polymer backbone.[28] These polymers exhibited effective low-fouling performance against various charged proteins and both passive and active marine foulers in laboratory experiments.

Despite being potential candidates as anti-fouling reagents, studies on the hydration and anti-icing behaviors of various zwitterionic polymers remain limited.[29–33] Chen investigated the *in situ* surface hydration of polyCBAA and polySBMA polymers employing sum frequency generation (SFG) vibrational spectroscopy.[29] Song *et al.* explored the correlation between the material composition and structural features of CBMA, SBMA, and MPC zwitterionic polymer brushes in preventing protein adhesion through molecular dynamics (MD) simulations.[31] Sarker *et al.* examined the hydration behavior of trimethylamine-*N*-oxide (TMAO) and CBs with varying charge-separation distances, employing *ab initio* MD simulations and SFG spectroscopy to investigate their anti-fouling properties.[32] In our previous work, density functional theory (DFT) was applied to study the hydration behaviors of two zwitterionic polymers, polySBMA and polyMPC, where intermolecular interactions with water have been evaluated.[33]

In this study, we have systematically investigated the molecular-level interactions of four zwitterionic polymers: poly(sulfobetaine methacrylate) (polySB), poly(2-methacryloyloxyethyl phosphorylcholine) (polyMPC), poly(2-carboxy-*N*, *N*-dimethyl-*N*-(3′-acrylamidopropyl)) (polyCBAA), and polySBi with water and ice (Fig. 1). Each polymer contains distinct cationic and anionic moieties arranged in different positions within the polymer architecture. Due to their diverse chemical structures, they exhibit unique electronic properties. This study aims to examine how these structural differences, specifically, the positioning and nature of the charged groups, influence their interactions with water molecules, and consequently, their anti-icing properties. Previous studies have

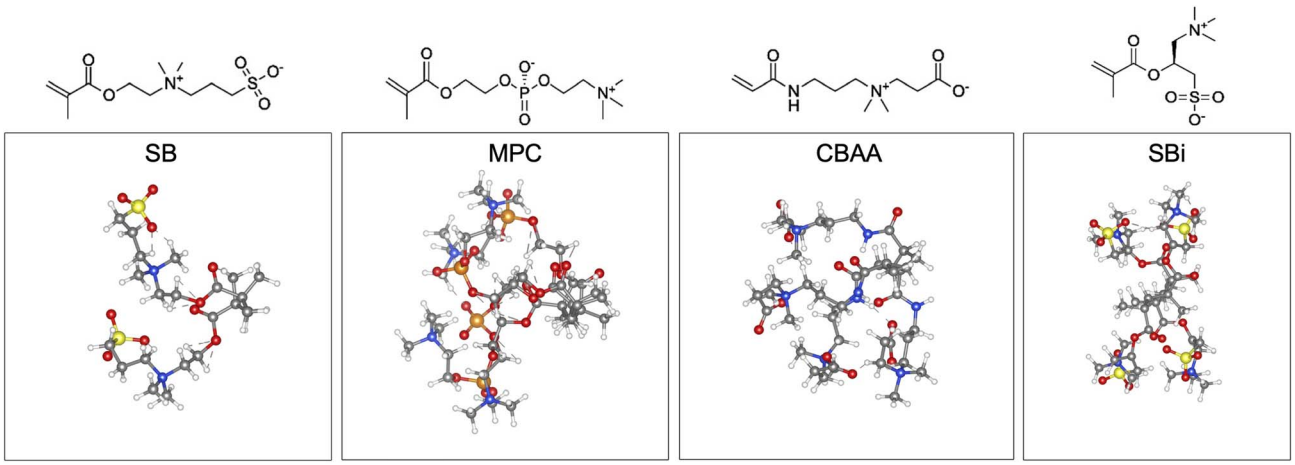

Fig. 1 Chemical and atomic structures of SB, MPC, CBAA, and SBi zwitterionic polymers.

Open Access Article. Published on 09 October 2025. Downloaded on 10/29/2025 11:21:30 PM. This article is licensed under a Creative Commons Attribution-NonCommercial 3.0 Unported Licence.

shown that polySB and polyCBAA contain functional groups capable of forming strong hydrogen bonds with water, creating hydration layers that reduce ice adhesion and formation. In contrast, polyMPC which mimics the phospholipid head group in cell membranes, promotes stable water layers that act as barriers against protein and cell adhesion. Structurally, polySB and polyCBAA have terminal anionic moieties, while polyMPC features a terminal cationic group. Interestingly, in polySBi, the positions of the cationic and anionic groups relative to the polymer backbone have been altered compared to polySB. This unique arrangement allows us to examine how the varying segmental dipole orientation influences water–polymer interactions. Using plane-wave density functional theory (DFT), we investigated the intermolecular interactions between these zwitterionic polymers and water or ice. DFT calculations have proven to be highly effective in accurately predicting electronic structures and calculating interactions between adsorbates and adsorbents. The results obtained from our present study provide detailed insights into polymer–water/ice interactions at the molecular level, contributing valuable perspectives on hydration responses. This would serve as the foundation for advancing research to design anti-icing coatings using different zwitterionic polymers with a focus on both energy efficiency and sustainability.

Methods

In this study, the Vienna *Ab Initio* Simulation Package (VASP)[34–36] is used to perform non-spin-polarized planewave DFT calculations, where the core and valence electrons are described using the projector-augmented wave (PAW)[37,38] and the generalized-gradient approximation in the Perdew–Burke–Ernzerhof (PBE)[39] form is used to describe electron exchange and correlation. Dispersion interactions are incorporated using Grimme's PBE-D3 corrections with the Becke-Johnson damping function.[40] The kinetic energy cutoff is set to 400 eV, and a Gaussian smearing of 0.03 eV is applied for Brillouinzone integrations. The atomic positions are optimized using the conjugate-gradient method with energy and force tolerances of 10^{-6} eV and 0.01 eV Å^{-1}, respectively. These criteria ensure that geometry optimization leads to a fully relaxed structure corresponding to a local minimum on the potential energy surface. Initially, the electronic and chemical properties of all monomers in the gas phase are calculated using the Gaussian16 software package.[41] For this calculation, we used Becke's three-parameter hybrid functional (B3LYP)[42] with the Pople-type triple-zeta 6-311++G(d,p) basis set, which includes diffuse functions on all atoms and polarization functions on both heavy atoms and hydrogens.[43]

To model hydration and ice interaction, we employed 1D periodic models of a polymer chain consisting of four monomer units, surrounded by a vacuum to eliminate potential interactions between periodic replicas. The *x*-axis is defined to represent the polymer backbone. The monomeric units and atomic structures of the 3D periodic models for each polymer are shown in Fig. 1. To model fully hydrated chains, we packed the simulation cell with 70 H_2O molecules, resulting in a total density of about 0.96 g cm^{-3}, matching the target bulk water density at room temperature. To account for the variability in water positioning around the polymer, we created three different models for each polymer, each containing 70 randomly distributed water molecules. All dry and wet models are fully optimized to their ground state structures before conducting morphology and bonding analyses. To quantify the interaction strength, we calculated water adsorption energies using the following equation (eqn (1))

$$E_{\mathrm{ads}} = (E_{\mathrm{poly+adsorbate}} - E_{\mathrm{poly}} - n \times E_{\mathrm{adsorbate}})/n \tag{1}$$

where E_{ads} is the adsorption energy, $E_{\mathrm{poly+adsorbate}}$ is the energy of the polymer with the adsorbate bonded to it, which can be H_2O molecules or ice cluster, E_{poly} is the energy of the dry polymer chain, $E_{\mathrm{adsorbate}}$ is the energy of a free water molecule or ice cluster, and n equals the number of water molecules per simulation cell or equals 1 in the case of ice cluster. A negative adsorption energy indicates an attractive interaction between the polymer and the adsorbate. It is worth mentioning that the E_{ads} includes the change in energy due to polymer–polymer, water–polymer, and water–water interaction. The more negative the adsorption energy, the stronger the attraction between the polymer and water, corresponding to a higher hydration capability of the polymer. To ensure consistent comparison across different polymer systems, the number of water molecules n is set as 70; this value of n, along with the chosen simulation cell sizes, ensures that most water molecules remain within the interaction range of the polymers, specifically within the nearest and second nearest hydration shells. We also calculated ice cluster formation energy $E_{\mathrm{form}} = E_{n\mathrm{H_2O}}^{\mathrm{ice}} - E_{n\mathrm{H_2O}}^{\mathrm{liquid}}$ to further test the hypothesis that the strongly bonded dynamic hydration layer will not likely freeze. Such that, E_{form} is calculated as the energy difference of the system of $n\mathrm{H_2O}$ ice cluster adsorbed on the polymer relative to the same number of adsorbed liquid like water molecules, where $E_{n\mathrm{H_2O}}^{\mathrm{liquid}}$ is the total energy of the polymer with n adsorbed water molecules and $E_{n\mathrm{H_2O}}^{\mathrm{ice}}$ is the total energy of the system with adsorbed ice cluster.

Furthermore, to characterize the electronic structure of the system, we analyzed the electron density of states (DOS), which provides a quantitative measure of the number of states within specific energy ranges. The Bader method is used to perform a partial charge analysis of all atoms for the optimized ground-state structures.[44–47] The Bader electron population of an atom ($Q_{\mathrm{A}}^{\mathrm{Bader}}$) is calculated as the integral of the electron density ($\rho(r)$) over the atomic basin (Ω_{A}): $Q_{\mathrm{A}}^{\mathrm{Bader}} = \int_{\Omega_{\mathrm{A}}} \rho(r)\mathrm{d}r$. Additionally, to provide a detailed picture of the nature of the bond between water and polymer, charge density and chemical bonding analyses are performed using the Crystal Orbital Hamilton population (COHP) method,[48] employing the local orbital basis suite towards electronic-structure reconstruction (LOBSTER) code.[49]

Results and discussions

Electronic properties of zwitterionic polymers

We first calculated the electronic properties of the four studied zwitterionic polymers in their dry state at their ground-state

Open Access Article. Published on 09 October 2025. Downloaded on 10/29/2025 11:21:30 PM.
This article is licensed under a Creative Commons Attribution-NonCommercial 3.0 Unported Licence.

Table 1 Electronic properties of zwitterionic polymers

Monomer (unit)	HOMO (eV)	LUMO (eV)	Polarizability (α) (Bohr^3)	Electrophilicity[50] (ω) (eV)	Electronegativity[50] (χ) (eV)	Dipole moment (μ) (Debye)
SB	−5.9	−2.9	174.6	3.2	4.4	14.2
MPC	−6.2	−1.5	181.7	1.5	3.8	15.2
CBAA	−6.1	−2.5	157.8	2.6	4.3	12.9
SBi	−5.5	−2.9	164.8	3.5	4.2	20.4

configuration. Fig. 1 illustrates the chemical and atomic structures of the four polymers. As shown in Table 1, MPC exhibits the highest polarizability (181.7 Bohr^3) along with the lowest electrophilicity (1.5 eV) and electronegativity (3.8 eV) values, whereas CBAA follows the opposite trend, displaying the lowest polarizability and the highest electrophilicity and electronegativity values. SB and SBi fall in between MPC and CBAA concerning these properties. Considering the dipole moment alone, the observed trend is: SBi > MPC > SB > CBAA. A polymer characterized by high polarizability, low electrophilicity and electronegativity, and a significant dipole moment is expected to exhibit greater hydration due to its strong interactions with adsorbates (here, water) and enhanced charge transfer from the polymer to water. However, electronic properties alone cannot provide accurate predictions, they offer only an initial assumption. A more comprehensive analysis incorporating both structural and electronic factors is essential to accurately capture the interactions between polymers and water or ice, as demonstrated by the results of this study.

The polymers' electronic properties directly influence their ability to form hydrogen bonds with water and their overall hydration behavior. Thus, we calculated the electronic structure and density of states (DOS) of each of the polymers. Fig. 2a presents the DOS plots for all four polymers. The DOS of a polymer indicates the number of electronic states available at each energy level for electron occupancy. The Fermi level represents the highest energy level an electron can occupy at absolute zero temperature. A higher DOS intensity at the Fermi level suggests a greater number of free electrons, increasing the polymer's tendency to interact with adsorbates. For polyMPC, an intensely occupied Fermi level of 6.3 states per eV is observed, compared to 4.8 states per eV for polySB and 2.3 states per eV for CBAA. These states, primarily originate from oxygen p orbitals of the anionic group, facilitating orbital overlaps with adsorbates. This suggests that adsorbate (here, water) can form strong bonds with these zwitterionic polymers, particularly with polyMPC. Our previous work demonstrated very strong hydrogen bonding between polyMPC and water molecules.[37] In contrast, although polySBi has the highest number of states at the Fermi level, they are unoccupied, indicating its stronger electron-accepting character compared to the other polymers. Now, during polymer–water interactions, electron transfer typically occurs from the polymer to water. Since due to the presence of vacant energy states at Fermi level, polySBi cannot readily donate electrons; thus, this transfer is limited.

In Fig. 2b, we evaluated the HOMO–LUMO energy levels of water and the polymers studied. The calculated HOMO and LUMO energies of the monomers are compared with the water molecule. Notably, water has a lower HOMO level than all the polymers studied, suggesting the possibility of a potential electron transfer from the polymer to water. The observed trend in HOMO energy levels is as follows: SBi has the highest energy

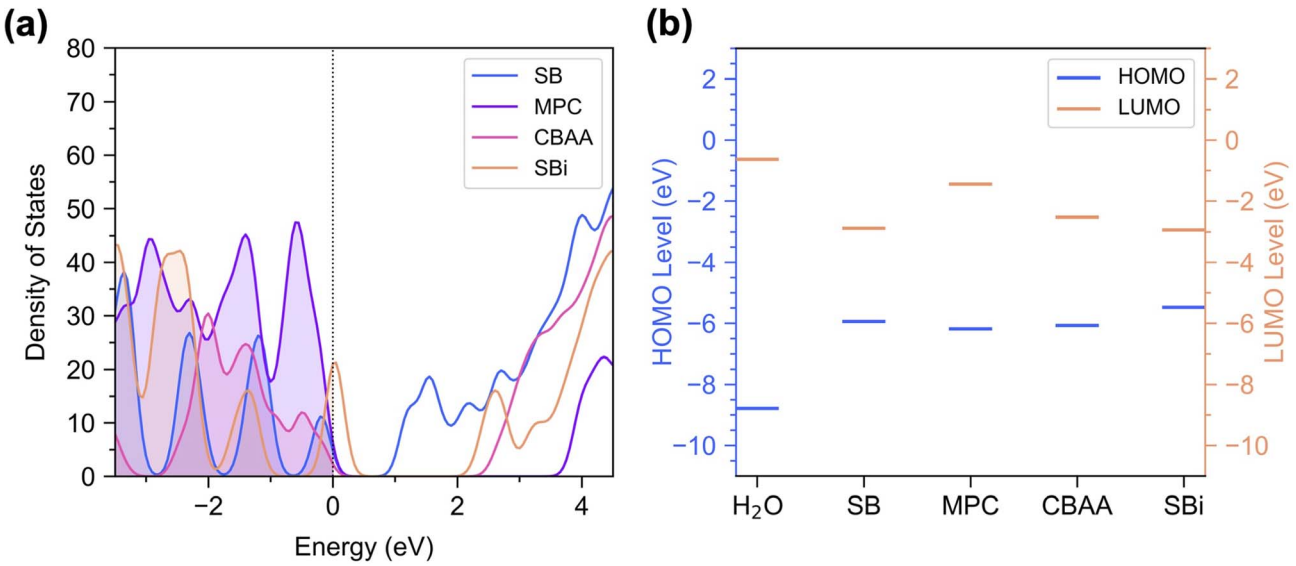

Fig. 2 Electronic properties of zwitterionic polymers: (a) total electronic density of states of the four polymers. (b) Calculated HOMO–LUMO energy levels *vs.* vacuum.

 This journal is © The Royal Society of Chemistry 2025

Open Access Article. Published on 09 October 2025. Downloaded on 10/29/2025 11:21:30 PM. This article is licensed under a Creative Commons Attribution-NonCommercial 3.0 Unported Licence.

HOMO level (−5.5 eV) and the smallest band gap, followed by SB (−5.9 eV), while CBAA and MPC exhibit the lowest energy HOMO levels at −6.1 eV and −6.2 eV, respectively. However, the HOMO levels of the polymers align almost on the same energy scale and do not indicate any specific preference among the polymers for interacting more with water.

Conformational analysis of polymers in dry and wet conditions

After adding water molecules to the model/polymer, we next compared the polymer segmental structures under dry and wet conditions. In this analysis, we compared two key angles: the dipole–dipole angle and the side-chain angle. The dipole–dipole angle is defined as the angle between the center of mass of the ionic groups, represented by A and C, and the carbon atom of the central $-CH_2-$ group connecting the ionic groups, as illustrated in Fig. 3(a) (top). The side-chain angle is defined as the angle between the carboxylic oxygen (A) and the center of mass of the ionic moieties (B and C) as shown in Fig. 3(a) (bottom). Overall, the results indicate conformational changes upon hydration, suggesting stronger intermolecular interactions. In terms of dipole–dipole and side-chain angles, the angles generally increase from dry to wet conditions, except for the CBAA polymer, which suggests a slight flattening of the polymer in the wet state. Additionally, for CBAA, the large error bars in determining both angles indicate greater dynamic behavior in water. Across all polymers studied, the internal hydrogen bond lengths between side chains decrease upon hydration. The side-chain lengths show elongation for MPC and CBAA, while SB and SBi exhibit almost no change when transitioning from dry to wet conditions. The overlapping error bars between dry and wet conditions suggest that some of these conformational changes may not be statistically significant. This could be due to the relatively small model used in this study, and a larger model might amplify these changes. However, increasing the model size would have required simplifying the computational method, potentially compromising the accuracy of the results. Therefore, we opted for a balanced approach using a four monomer chain to ensure both computational feasibility and reliable results.

Water adsorption and polymer hydration

In this section, we discuss the interaction between polymers and adsorbed water molecules. As mentioned in the Methods section, each simulation cell contains 70 water molecules to maintain the cell density ∼0.96 gm cm^{-3}. Fig. 4a presents the optimized

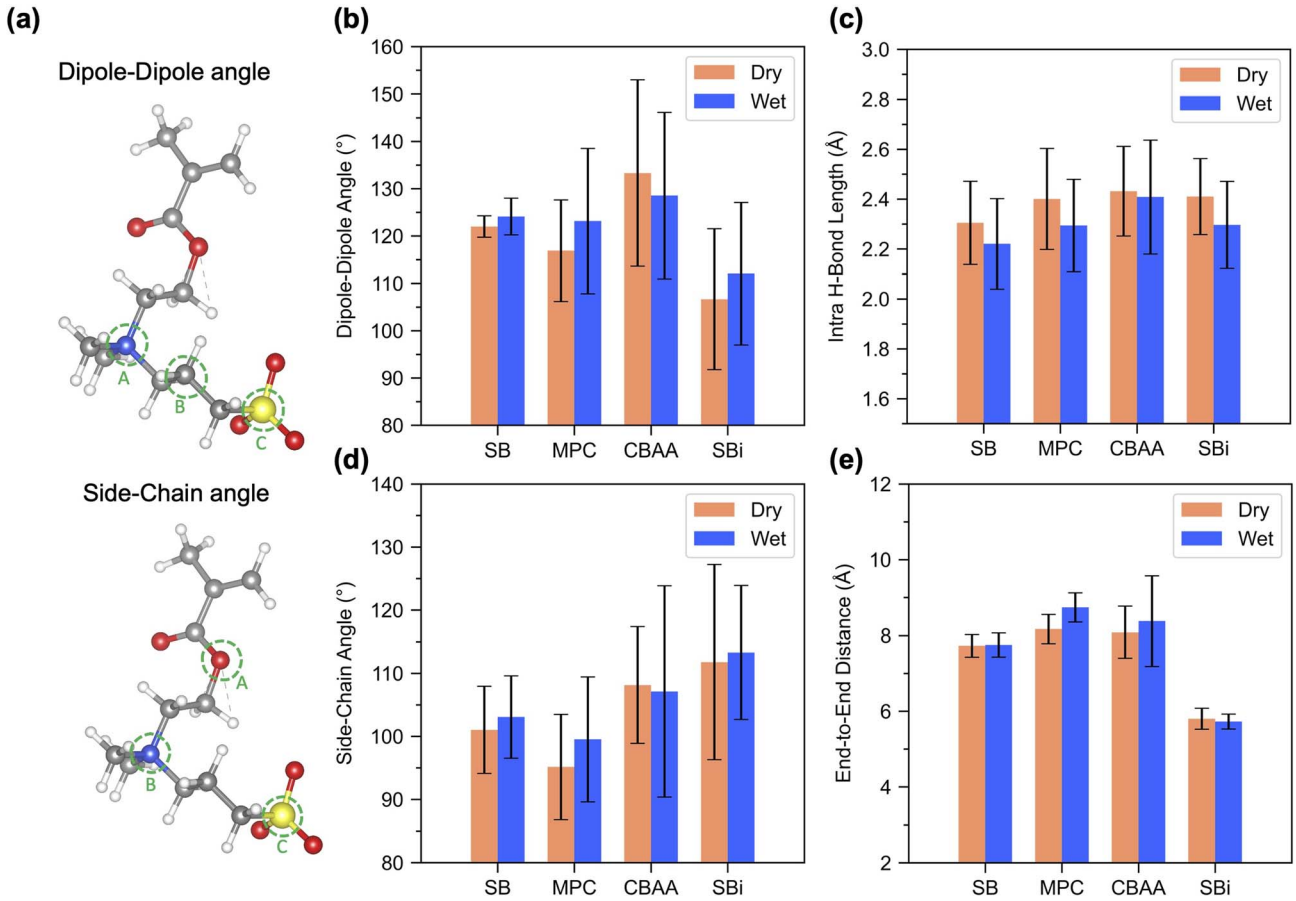

Fig. 3 Comparison of geometric parameters of zwitterionic polymers under dry and wet conditions: (a) schematic illustration defining dipole–dipole and side-chain angle measurements, (b) variation in dipole–dipole angles, (c) changes in intramolecular hydrogen bond lengths between polymer side chains, (d) variation in side-chain angles, and (e) changes in end-to-end distances. Error bars represent standard deviations from the simulations.

Open Access Article. Published on 09 October 2025. Downloaded on 10/29/2025 11:21:30 PM.
This article is licensed under a Creative Commons Attribution-NonCommercial 3.0 Unported Licence.

ground-state geometries of all four wet polymers. It is important to note that the calculated adsorption energy accounts for polymer–water interactions, polymer–polymer interactions, and water–water interactions. The polymer–water interaction exhibits varying binding strengths across the different polymers studied. Quantitative evidence of these interactions is provided by the water adsorption energy per water molecule (Fig. 4b), the net H_2O Bader charge (Fig. 4c), and Integrated Crystal Orbital Hamilton Population (-ICOHP) analyses (Fig. 4d). From optimized geometries, it is evident that the water molecules interact with the polymers primarily through hydrogen bonding. In all models, it is evident that polyCBAA accommodates 2–3 more water molecules than the other three polymers. This suggests that polyCBAA has a larger accessible surface area, allowing it to bind more water molecules, which is consistent with the increase in end-to-end distances observed when transitioning from the dry to the wet model. Regarding water adsorption energy, polyCBAA exhibits the highest adsorption energy, followed by polySB, polyMPC, and the lowest for polySBi. The strong adsorption energy of polyCBAA can be attributed to two factors: the higher charge density of its anionic group compared to polySB and its interaction with a greater number of water molecules, which increases the total adsorption energy and, consequently, the adsorption energy per water molecule. In the case of polyMPC, the anionic group is embedded within the side chain, whereas in polyCBAA and polySB, it is positioned at the terminal end. This difference in placement likely contributes to the lower adsorption energy observed for polyMPC. For polySBi, the adsorption energy is the lowest among all, likely due to weaker hydrogen bonding between the polymer and water molecules, as predicted by DOS and HOMO–LUMO analyses. Furthermore, we have calculated the DOS of wet systems after water adsorption, with the corresponding data presented in Fig. S1 and Table S1 in SI. The results show a decrease in the DOS intensity at the Fermi level for polyMPC, polySB, and polyCBAA after water adsorption. As previously noted, a higher DOS intensity at the Fermi level corresponds to a greater number of free electrons. Therefore, the observed reduction in DOS intensity upon hydration suggests charge transfer from these polymers to the adsorbed water molecules. In contrast, polySBi exhibits almost no change at the Fermi level, suggesting minimal interaction with water. This observation is consistent with the adsorption energy analysis and will be further supported by the Bader charge analysis discussed later. Additionally, a notable upward shift in the conduction band maximum (CBM) is observed for polySB and polyCBAA. This shift may result from structural deformation upon hydration, which alters orbital overlap and elevates conduction states, thereby pushing the conduction band to higher energies.

In terms of net H_2O Bader charge, calculated as the sum of the charges of all 70 water molecules within the simulation cell, polyCBAA exhibits the highest charge transfer, followed by polyMPC, polySB, and the least for polySBi, as shown in Fig. 4c. The -ICOHP analysis, which measures bonding strength by assessing the bonding orbital overlap between the adsorbate

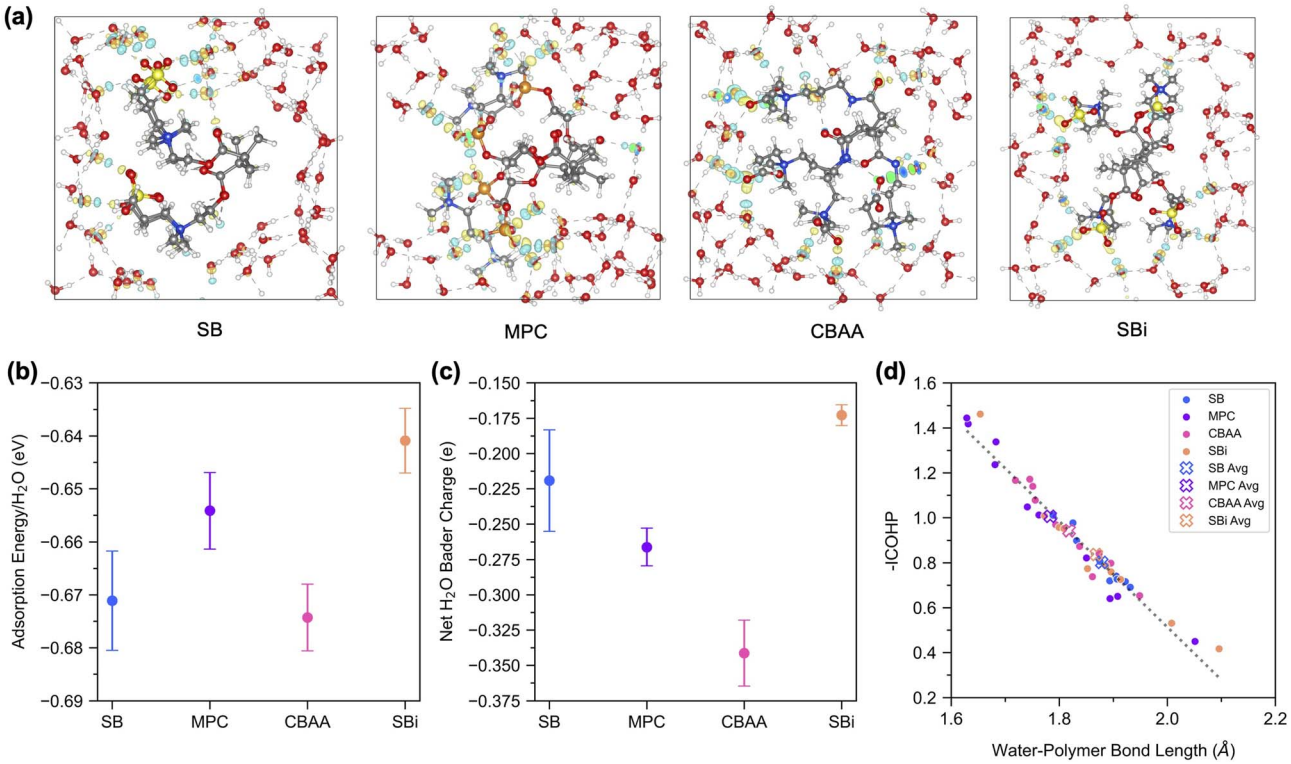

Fig. 4 Characterization of polymer–water interactions in different polymer materials. (a) Molecular visualization of the charge density difference of the wet polymer for each material. (b) Water adsorption energy per water molecule and (c) net H_2O Bader charge across the materials, showing varying degrees of polymer–water interaction strength. (d) Correlation between -ICOHP (Integrated Crystal Orbital Hamilton Population) and polymer–water bond length for polySB, polyMPC, polyCBAA, and polySBi polymers, with averaged values shown as crosses.

Open Access Article. Published on 09 October 2025. Downloaded on 10/29/2025 11:21:30 PM.
This article is licensed under a Creative Commons Attribution-NonCommercial 3.0 Unported Licence.

and adsorbent, along with polymer–water bond lengths, shows that polyMPC exhibits the highest -ICOHP value corresponding to the shortest bond to the adsorbed water molecules, indicating the strongest interaction (Fig. 4d). However, in the case of polyCBAA, a greater number of water molecules interact with the polymer, leading to higher water adsorption energy and charge transfer compared to other polymers. In the case of polySBi, the weakest interaction between polymer and water molecules among all is further confirmed by the lowest net H_2O Bader charge. Considering all three outcomes, it can be stated that polyMPC forms stronger interactions with water molecules by creating a tightly bonded hydration layer, while polyCBAA can interact with more water molecules with slightly weaker bonding, which may suggest the formation of a thicker hydration layer. Therefore, by considering the diversity of ionic groups, their orientation, and their placement relative to the polymer backbone, we analyzed the polymer–water interactions and found them to be most favorable for polyMPC, followed by polyCBAA and polySB, and least favorable for polySBi.

We have further analyzed the water structures after adsorption and compared their structural parameters, including O–H bond lengths, HOH angles, and water–water hydrogen bond distances, to three different ice configurations: ice prism, ice having 10-H_2O, and ice-Ih. These variations in water's molecular geometry and interactions serve as an indicator of the transition from liquid water to ice-like structures. Fig. S2 illustrates the changes in water's structural parameters relative to these ice configurations, while Table S2 presents ice similarity scores across different materials, which show how polymeric environments influence water structure and behavior.

Among the four polymers studied, polyMPC exhibits the highest overall ice similarity score of 8.92%, with a particularly strong contribution from hydrogen bond similarity (5.89%). In terms of O–H bond similarity, polyCBAA and polyMPC exhibit similar scores, both lower than that of polySB, further suggesting stronger interactions of polyCBAA and polyMPC with water than with polySB. Notably, all polymers exhibit relatively high HOH angle similarities (~17–18%) compared to other metrics. In the case of polySBi, although it exhibits the lowest overall ice similarity score, including the lowest values for most individual water structural parameters, this does not necessarily indicate that polySBi has better anti-icing properties. Moreover, the similarity scores obtained from our analysis indicate that all polymers have relatively low overall similarity scores (<9.0%), with minimal variations among them. These small differences can be attributed to water deformation caused by polymer–water interactions. Therefore, ice similarity scores may not be the most reliable metric here for ranking anti-icing performance. This limitation arises from our current DFT model size and may be addressed by studying larger polymer models through molecular dynamics simulations, which could also capture the impact of polymer configuration not considered here.

Polymer interactions with ice

In this section, we first examined the interactions of two different ice clusters: ice prism and ice-10H_2O with the four polymers. The optimized structures for ice prism interacting with the polymers (Fig. S3) reveal significant deformation of the ice clusters upon interaction with polySB and polyCBAA, as supported by RMSD values. Similarly, for ice-10H_2O (Fig. 5),

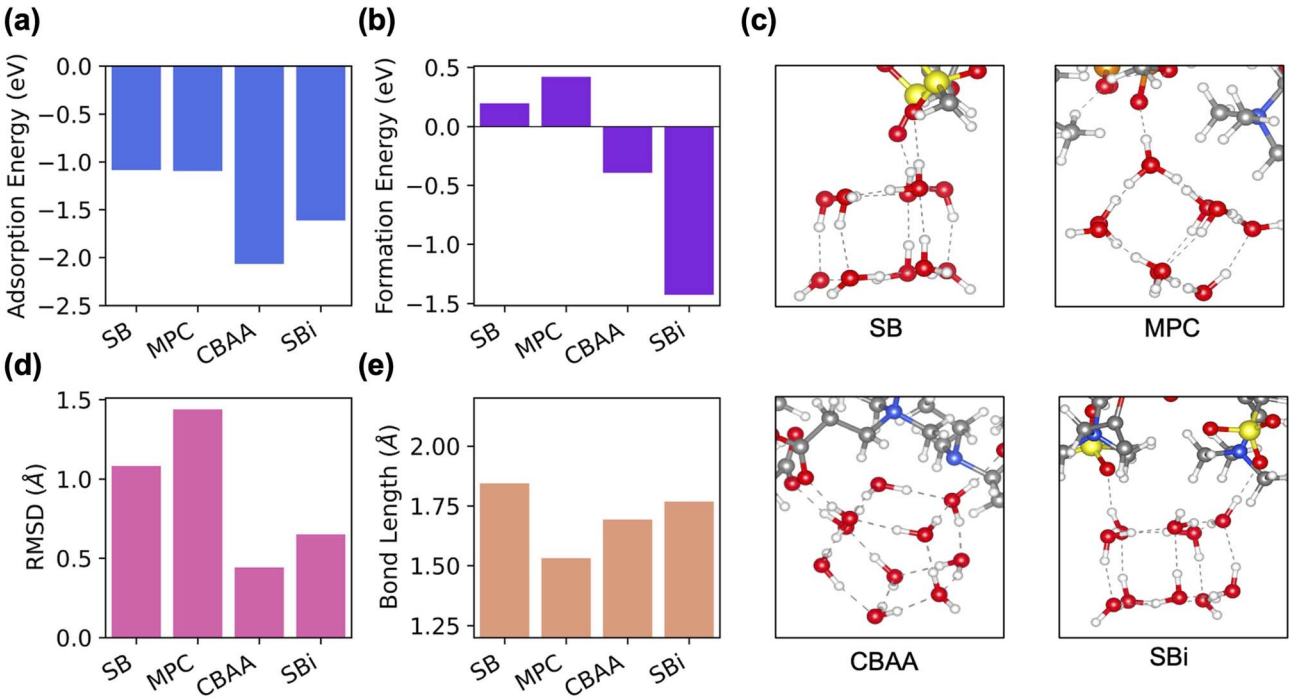

Fig. 5 (a) Calculated adsorption energy (eV) of 10-H_2O ice cluster on the polymer. (b) Formation energy (eV) from liquid water molecules to ice cluster. (c) Optimized molecular structures of the cluster on all four polymers, where the dashed-dotted line indicates hydrogen bonds. (d) Root means square deviation (RMSD) values (Å) quantifying structural variability. (e) Shortest polymer-cluster bond lengths (Å).

Open Access Article. Published on 09 October 2025. Downloaded on 10/29/2025 11:21:30 PM.
This article is licensed under a Creative Commons Attribution-NonCommercial 3.0 Unported Licence.

structural deformation is observed in the cases of polySB and polyMPC, which is also evident from RMSD measurements. The formation energy analysis shows that polySBi exhibits the most negative value, indicating the strongest interaction with ice-10H_2O, while polyCBAA shows a less negative formation energy. In contrast, for polySB and polyMPC, the substantial deformation of ice clusters and the positive formation energy suggest weaker interactions between these polymers and ice. This suggests that forming a perfect ice cluster in the first hydration layer is not energetically favorable for polySB and polyMPC. As a result, the ice clusters undergo deformation for polySB and polyMPC and behave more like liquid water, effectively acting as a self-lubricating interfacial layer. Additionally, polySBi exhibits reduced hydrophilicity compared to polySB, highlighting the critical role of charged group arrangements in determining molecular properties.

Understanding the ice adhesion properties of polymers is crucial, as these directly influence the interfacial interactions between ice and potential anti-icing materials. To investigate the adsorption mechanisms of the four selected zwitterionic polymers on ice surfaces, we performed a comprehensive analysis of surface planes of the hexagonal ice (ice-Ih) crystal. Specifically, we geometry-optimized the primary (001) surface plane of ice-Ih to serve as the model surface for subsequent ice adsorption/adhesion evaluations.

We analyzed the ice adhesion capability of the four polymers using the ice (001) surface. We considered two different mechanisms: in one, the ice surface was fixed while only the polymer was allowed to relax, and in the other, both the ice surface and the polymer were fully relaxed. In agreement with our previous findings, MPC (then SB) has the shortest polymer–water bond in the relaxed surface models (Fig. 6a), which indicates stronger water–polymer interaction. As shown in Fig. 6c, for the fixed surface calculation, polySBi exhibits the lowest adsorption energy among all the polymers. In the case of the relaxed surface calculation, while polySBi still has relatively low adsorption energy, the other three polymers show significantly higher adsorption energies.

To understand the structural changes of the surface after adsorption, we further calculated the surface deformation energy following adsorption. In Fig. 6d, polyCBAA exhibits the highest surface deformation energy, followed by polyMPC, polySB, and finally polySBi, which has the least surface deformation. This indicates that for polyCBAA, polyMPC, and polySB, the ice surface undergoes substantial deformation, behaving more like lubricating water molecules. Since these polymers

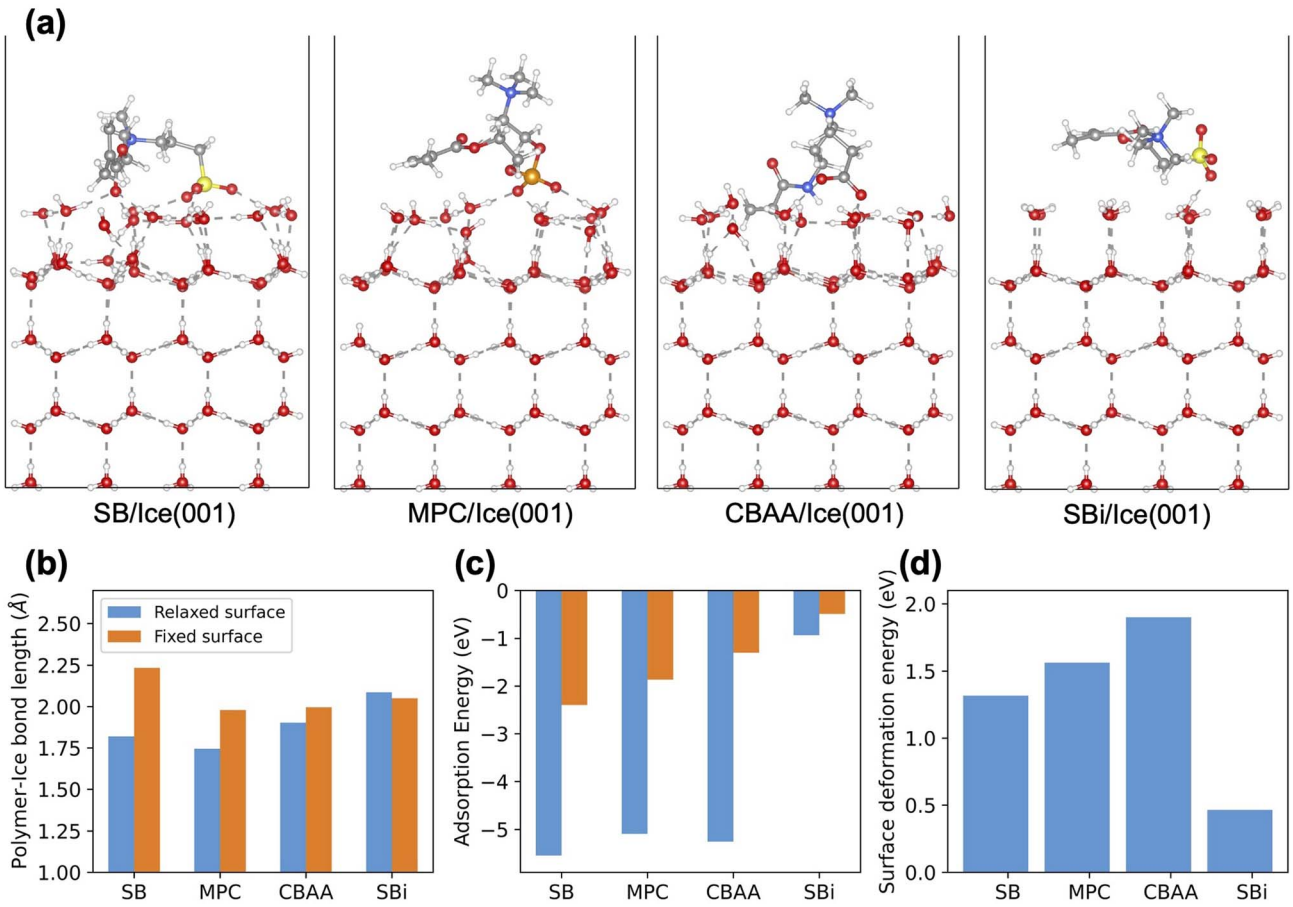

Fig. 6 (a) Optimized structures of four zwitterionic monomers (SB, MPC, CBAA, and SBi) adsorbed on the (001) ice surface. (b) Comparison of polymer–ice bond lengths (Å) for both relaxed (blue) and fixed (orange) ice surfaces across the four monomers. (c) Adsorption energies (eV) of the monomers on relaxed (blue) and fixed (orange) ice surfaces. (d) Surface deformation energies (eV) induced by monomer adsorption.

 This journal is © The Royal Society of Chemistry 2025

Open Access Article. Published on 09 October 2025. Downloaded on 10/29/2025 11:21:30 PM.
This article is licensed under a Creative Commons Attribution-NonCommercial 3.0 Unported Licence.

strongly interact with water molecules, after surface deformation, they strongly interact with lubricating water molecules and thus exhibit high adsorption energy. Therefore, among the four polymers studied, although polySBi shows the lowest ice adhesion, in the presence of the other three polymers, the interface layer of ice loses its intrinsic properties and behaves more like a lubricating water surface.

Overall, polySB and polyMPC demonstrate better anti-icing and ice adhesion resistance, effectively preventing ice formation by disrupting ice cluster integrity and deforming the ice surface. While polyCBAA exhibits weak ice cluster binding, it shares similar ice surface deformation characteristics like polySB and polyMPC. Conversely, polySBi, despite having the lowest ice adhesion, displays the weakest anti-icing performance, as indicated by its most negative ice cluster formation energy, corroborating well with the low adsorption energy for water binding and lower polymer–water charge transfer as observed from our calculation. Thus, our findings suggest a possible trend in anti-icing and ice adhesion resistance, where polyMPC and polySB perform comparably, followed by polyCBAA and polySBi.

While the use of four monomer chains balances computational efficiency and accuracy, it may underestimate long-range electronic effects and conformational diversity. Nevertheless, the key local electronic interactions governing hydration behavior and ice interaction are well captured, and the observed trends are expected to persist for longer polymer chains. Since the anionic groups are directly involved in interactions with water molecules during hydration, our calculations reveal variations in interaction strength depending on the nature of these groups. In polyMPC, the central atom of the anionic group is phosphorus; in polyCBAA, it is carbon; and in polySB and polySBi, it is sulfur. Because phosphorus is less electronegative than carbon and sulfur, the oxygen atoms of the anionic groups are more electron-rich, enabling the most favorable interactions with water molecules. In contrast, the electronegativity difference between carbon and sulfur is relatively small; however, as mentioned earlier, the anionic group in polyCBAA, having a higher charge density than in polySB, interacts slightly more favorably with water. Additionally, the arrangement of side chains plays a crucial role in determining the polymer's hydrophilicity, which in turn affects hydration, as reflected by the lower hydration of polySBi relative to polySB. Therefore, a zwitterionic polymer featuring an anionic head with a less electronegative central atom and higher charge density, combined with an unbranched, hydrophilic side chain, is expected to be most effective for designing anti-icing polymers. These insights provide a more complete understanding of polymer–water and polymer–ice interactions which can serve as the foundation for designing effective anti-icing polymers. Furthermore, this study aligns closely with energy efficiency and sustainability goals, as zwitterionic polymer coatings are environmentally benign, require lower maintenance, offer potential cost and energy savings, therefore making them promising materials for sustainable, energy-efficient technologies.

Conclusion

In this study, we investigated the interactions of four zwitterionic polymers: polySB, polyMPC, polyCBAA, and polySBi with water and ice to assess their hydration and anti-icing properties using DFT calculations. Our results show that no single property solely dictates a polymer's hydration or anti-icing performance. Instead, a combination of electronic descriptors, adsorption energies, Bader charge, and polymer–water bonding strength offers a more complete picture. DOS calculations for dry polymers indicate that unlike polySBi, polyMPC, polySB, and polyCBAA have occupied states at the Fermi level, suggesting stronger electron-donating character and higher potential for water interaction, which is supported by wet system DOS results. Adsorption energy analysis shows that polyCBAA binds 2–3 more water molecules than the others, yielding the highest energy per water molecule. Bader analysis further confirms the highest net charge on water molecules near polyCBAA, followed by polyMPC. However, -ICOHP analysis reveals that polyMPC forms the shortest and strongest hydrogen bonds, with the highest -ICOHP value indicating greater orbital overlap between the polymer and water, resulting in a tightly bound hydration layer, while polyCBAA forms a thicker layer with slightly weaker bonding. Therefore, based on these analyses, the polymers can be ranked in terms of hydration capability as follows: polyMPC > polyCBAA ≥ polySB > polySBi.

Analysis of small ice cluster interactions reveals that polySB and polyMPC significantly deform the clusters, leading to positive formation energies, whereas polyCBAA shows slightly negative value and polySBi the most negative, indicating strong ice binding. Ice (001) surface adhesion studies further show notable surface deformation for polySB, polyMPC, and polyCBAA, suggesting water-like lubricity and anti-icing behavior. In contrast, polySBi exhibits low ice adhesion without surface deformation. Overall, polySB and polyMPC offer the best anti-icing performance by disrupting ice integrity and deforming the surface, polyCBAA shows moderate resistance with weaker ice binding, and polySBi performs the poorest due to strong ice interaction and minimal deformation. Based on our modeling analyses, the polymers appear to follow a possible trend in anti-icing and ice adhesion resistance, with polyMPC and polySB performing comparably, followed by polyCBAA and polySBi. Overall, this study enhances our understanding of how different zwitterionic polymers interact with water and ice at a fundamental molecular level.

Author contributions

Sara A. Tolba: methodology, software, formal analysis, validation, writing – review & editing. Tamalika Ash: formal analysis, validation, writing – original draft, writing – review & editing. Wenjie Xia: conceptualization, supervision, project administration, funding acquisition, resources, writing – review & editing.

Conflicts of interest

There are no conflicts to declare.

Open Access Article. Published on 09 October 2025. Downloaded on 10/29/2025 11:21:30 PM.
This article is licensed under a Creative Commons Attribution-NonCommercial 3.0 Unported Licence.

Data availability

The data supporting the findings of the study have been presented in the manuscript and supplementary information (SI). The data are available from the authors upon reasonable request. Supplementary information is available. See DOI: https://doi.org/10.1039/d5ta04860e.

Acknowledgements

The authors acknowledge the support from the U.S. Office of Naval Research (ONR) (Award No. 00014-22-1-2129 and 00014-24-1-2011). This work used the resources of the Center for Computationally Assisted Science and Technology (CCAST) at NDSU, which were made possible in part of NSF MRI (Award No. 2019077).

References

1 J. Xiao and S. Chaudhuri, Design of Anti-Icing Coatings Using Supercooled Droplets as Nano-to-Microscale Probes, *Langmuir*, 2012, **28**(9), 4434–4446, DOI: 10.1021/la2034565.

2 X. Yao, Y. Song and L. Jiang, Applications of Bio-Inspired Special Wettable Surfaces, *Adv. Mater.*, 2011, **23**(6), 719–734, DOI: 10.1002/adma.201002689.

3 O. Parent and A. Ilinca, Anti-Icing and de-Icing Techniques for Wind Turbines: Critical Review, *Cold Reg. Sci. Technol.*, 2011, **65**(1), 88–96, DOI: 10.1016/j.coldregions.2010.01.005.

4 A. G. Kraj and E. L. Bibeau, Phases of Icing on Wind Turbine Blades Characterized by Ice Accumulation, *Renew. Energy*, 2010, **35**(5), 966–972, DOI: 10.1016/j.renene.2009.09.013.

5 K. C. Jha, E. Anim-Danso, S. Bekele, G. Eason and M. Tsige, On Modulating Interfacial Structure towards Improved Anti-Icing Performance, *Coatings*, 2016, **6**(1), 3, DOI: 10.3390/coatings6010003.

6 L. Fay and X. Shi, Environmental Impacts of Chemicals for Snow and Ice Control: State of the Knowledge, *Water Air Soil Pollut.*, 2012, **223**, 2751–2770, DOI: 10.1007/s11270-011-1064-6.

7 J. Ayres, W. H. Simendinger and C. M. Balik, Characterization of Titanium Alkoxide Sol-Gel Systems Designed for Anti-Icing Coatings: I. Chemistry, *J. Coat. Technol. Res.*, 2007, **4**, 463–471, DOI: 10.1007/s11998-007-9054-8.

8 J. Ayres, W. H. Simendinger and C. M. Balik, Characterization of Titanium Alkoxide Sol-Gel Systems Designed for Anti-Icing Coatings: II. Mass Loss Kinetics, *J. Coat. Technol. Res.*, 2007, **4**, 473–481, DOI: 10.1007/s11998-007-9055-7.

9 R. Carriveau, A. Edrisy, P. Cadieux and R. Mailloux, Ice Adhesion Issues in Renewable Energy Infrastructure, *J. Adhes. Sci. Technol.*, 2012, **26**(4–5), 447–461, DOI: 10.1163/016942411X574592.

10 J. Lv, Y. Song, L. Jiang and J. Wang, Bio-Inspired Strategies for Anti-Icing, *ACS Nano*, 2014, **8**(4), 3152–3169, DOI: 10.1021/nn406522n.

11 J. T. Simpson, S. R. Hunter and T. Aytug, Superhydrophobic Materials and Coatings: A Review, *Rep. Prog. Phys.*, 2015, **78**(8), 086501, DOI: 10.1088/0034-4885/78/8/086501.

12 Y. Si and Z. Guo, Superhydrophobic Nanocoatings: From Materials to Fabrications and to Applications, *Nanoscale*, 2015, **7**(14), 5922–5946, DOI: 10.1039/c4nr07554d.

13 H. G. Yang, C. Ma, K. Y. Li, K. Liu, M. Loznik, R. Teeuwen, J. C. M. van Hest, X. Zhou, A. Herrmann and J. Wang, Tuning Ice Nucleation with Supercharged Polypeptides, *Adv. Mater.*, 2016, **28**(25), 5008–5012, DOI: 10.1002/adma.201600496.

14 D. Ehre, E. Lavert, M. Lahav and I. Lubomirsky, Water Freezes Differently on Positively and Negatively Charged Surfaces of Pyroelectric Materials, *Science*, 2010, **327**(5966), 672–675, DOI: 10.1126/science.1178085.

15 P. Guo, Y. Zheng, M. Wen, C. Song, Y. Lin and L. Jiang, Icephobic/Anti-Icing Properties of Micro/Nanostructured Surfaces, *Adv. Mater.*, 2012, **24**(19), 2642–2648, DOI: 10.1002/adma.201104412.

16 L. Wang, Q. Gong, S. Zhan, L. Jiang and Y. Zheng, Robust Anti-Icing Performance of a Flexible Superhydrophobic Surface, *Adv. Mater.*, 2016, **28**(35), 7729–7735, DOI: 10.1002/adma.201602480.

17 X. Sun and K. Rykaczewski, Suppression of Frost Nucleation Achieved Using the Nanoengineered Integral Humidity Sink Effect, *ACS Nano*, 2017, **11**(1), 906–917, DOI: 10.1021/acsnano.6b07505.

18 C. Tao, S. Bai, X. Li, C. Li, L. Ren, Y. Zhao and X. Yuan, Formation of Zwitterionic Coatings with an Aqueous Lubricating Layer for Antifogging/Anti-Icing Applications, *Prog. Org. Coat.*, 2018, **115**, 56–64, DOI: 10.1016/j.porgcoat.2017.11.002.

19 B. Liang, G. Zhang, Z. Zhong, Y. Huang and Z. Su, Superhydrophilic Anti-Icing Coatings Based on Polyzwitterion Brushes, *Langmuir*, 2019, **35**(5), 1294–1301, DOI: 10.1021/acs.langmuir.8b01009.

20 S. Bai, X. Li, R. Zhang, C. Li, K. Zhu, P. Sun, Y. Zhao, L. Ren and X. Yuan, Enhancing Antifogging/Frost-Resisting Performances of Amphiphilic Coatings via Cationic, Zwitterionic or Anionic Polyelectrolytes, *Chem. Eng. J.*, 2019, **357**, 667–677, DOI: 10.1016/j.cej.2018.09.177.

21 Y. Wang, C. Chen, X. Wu, Z. Wang, S. Wen, J. Yu, C. Yan and W. Cong, Improved Antibiofouling Properties of Photobioreactor with Amphiphilic Sulfobetaine Copolymer Coatings, *Prog. Org. Coat.*, 2020, **144**, DOI: 10.1016/j.porgcoat.2020.105666.

22 K. Ishihara, N. P. Ziats, B. P. Tierney, N. Nakabayashi and J. M. Anderson, Protein Adsorption from Human Plasma Is Reduced on Phospholipid Polymers, *J. Biomed. Mater. Res.*, 1991, **25**(11), 1397–1407, DOI: 10.1002/jbm.820251107.

23 Y. Zhang, Y. Liu, B. Ren, D. Zhang, S. Xie, Y. Chang, J. Yang, J. Wu, L. Xu and J. Zheng, Fundamentals and Applications of Zwitterionic Antifouling Polymers, *J. Phys. D: Appl. Phys.*, 2019, **52**(40), 403001, DOI: 10.1088/1361-6463/ab2cbc.

24 W. Feng, J. Brash and S. Zhu, Atom-Transfer Radical Grafting Polymerization of 2-Methacryloyloxyethyl Phosphorylcholine from Silicon Wafer Surfaces, *J. Polym.*

 This journal is © The Royal Society of Chemistry 2025

Open Access Article. Published on 09 October 2025. Downloaded on 10/29/2025 11:21:30 PM.
This article is licensed under a Creative Commons Attribution-NonCommercial 3.0 Unported Licence.

Sci., Part A: Polym. Chem., 2004, **42**(12), 2931–2942, DOI: 10.1002/pola.20095.

25 Q. Shao and S. Jiang, Molecular Understanding and Design of Zwitterionic Materials, *Adv. Mater.*, 2015, **27**(1), 15–26, DOI: 10.1002/adma.201404059.

26 J. Zhang, L. Chen, L. Chen, S. Qian, X. Mou and J. Feng, Highly Antifouling, Biocompatible and Tough Double Network Hydrogel Based on Carboxybetaine-Type Zwitterionic Polymer and Alginate, *Carbohydr. Polym.*, 2021, **257**, 117627, DOI: 10.1016/j.carbpol.2021.117627.

27 C. Hua, Z. Li, K. Chen, L. Sun, L. Yu and X. Guo, Tunable Protein Adsorption by Zwitterionic Spherical Poly(CBAA) Brushes Prepared via Photoemulsion Polymerization, *Ind. Eng. Chem. Res.*, 2022, **61**(12), 4460–4468, DOI: 10.1021/acs.iecr.2c00075.

28 E. Schönemann, J. Koc, N. Aldred, A. S. Clare, A. Laschewsky, A. Rosenhahn and E. Wischerhoff, Synthesis of Novel Sulfobetaine Polymers with Differing Dipole Orientations in Their Side Chains, and Their Effects on the Antifouling Properties, *Macromol. Rapid Commun.*, 2020, **41**(1), 1900447, DOI: 10.1002/marc.201900447.

29 Z. Chen, Surface Hydration and Antifouling Activity of Zwitterionic Polymers, *Langmuir*, 2022, **38**(15), 4483–4489, DOI: 10.1021/acs.langmuir.2c00512.

30 D. Christiansen, G. Cheng and S. Mehraeen, Hydration and Ion Interactions of Zwitterionic Homopolymers with Varying Carbon Spacer Lengths, *Chem. Eng. Res. Des.*, 2022, **186**, 174–183, DOI: 10.1016/j.cherd.2022.07.032.

31 X. Song, J. Man, Y. Qiu, J. Wang, R. Li, Y. Zhang, G. Cui, J. Li, J. Li and Y. Chen, Study of Hydration Repulsion of Zwitterionic Polymer Brushes Resistant to Protein Adhesion through Molecular Simulations, *ACS Appl. Mater. Interfaces*, 2024, **16**(14), 17145–17162, DOI: 10.1021/acsami.3c18546.

32 P. Sarker, T. Lu, D. Liu, G. Wu, H. Chen, M. S. J. Sajib, S. Jiang, Z. Chen and T. Wei, Hydration Behaviors of Nonfouling Zwitterionic Materials, *Chem. Sci.*, 2023, **14**(27), 7500–7511, DOI: 10.1039/d3sc01977b.

33 S. A. Tolba and W. Xia, Molecular Insights into the Hydration of Zwitterionic Polymers, *Mol. Syst. Des. Eng.*, 2023, **8**(8), 1040–1048, DOI: 10.1039/d3me00020f.

34 G. Kresse and J. Furthmüller, Efficient Iterative Schemes for Ab Initio Total-Energy Calculations Using a Plane-Wave Basis Set, *Phys. Rev. B*, 1996, **54**(16), 11169–11186, DOI: 10.1103/PhysRevB.54.11169.

35 G. Kresse and J. Hafner, Ab Initio Molecular Dynamics for Liquid Metals, *Phys. Rev. B*, 1993, **47**(1), 558–561, DOI: 10.1103/PhysRevB.47.558.

36 G. Kresse and J. Furthmüller, Efficiency of Ab-Initio Total Energy Calculations for Metals and Semiconductors Using a Plane-Wave Basis Set, *Comput. Mater. Sci.*, 1996, **6**(1), 15–50, DOI: 10.1016/0927-0256(96)00008-0.

37 P. E. Blöchl, Projector Augmented-Wave Method, *Phys. Rev. B*, 1994, **50**(24), 17953–17979, DOI: 10.1103/PhysRevB.50.17953.

38 G. Kresse and D. Joubert, From Ultrasoft Pseudopotentials to the Projector Augmented-Wave Method, *Phys. Rev. B*, 1999, **59**(3), 1758–1775, DOI: 10.1103/PhysRevB.59.1758.

39 J. P. Perdew, K. Burke and M. Ernzerhof, Generalized Gradient Approximation Made Simple, *Phys. Rev. Lett.*, 1996, **77**(18), 3865–3868, DOI: 10.1103/PhysRevLett.77.3865.

40 S. Grimme, J. Antony, S. Ehrlich and H. Krieg, A Consistent and Accurate Ab Initio Parametrization of Density Functional Dispersion Correction (DFT-D) for the 94 Elements H-Pu, *J. Chem. Phys.*, 2010, **132**(15), 154104, DOI: 10.1063/1.3382344.

41 M. J. Frisch, G. W. Trucks, H. B. Schlegel, G. E. Scuseria, M. A. Robb, J. R. Cheeseman, G. Scalmani, V. Barone, G. A. Petersson, H. Nakatsuji, X. Li, M. Caricato, A. V. Marenich, J. Bloino, B. G. Janesko, R. Gomperts, B. Mennucci, H. P. Hratchian, J. V. Ortiz, A. F. Izmaylov, J. L. Sonnenberg, D. Williams-Young, F. Ding, F. Lipparini, F. Egidi, J. Goings, B. Peng, A. Petrone, T. Henderson, D. Ranasinghe, V. G. Zakrzewski, J. Gao, N. Rega, G. Zheng, W. Liang, M. Hada, M. Ehara, K. Toyota, R. Fukuda, J. Hasegawa, M. Ishida, T. Nakajima, Y. Honda, O. Kitao, H. Nakai, T. Vreven, K. Throssell, J. A. Montgomery Jr, J. E. Peralta, F. Ogliaro, M. J. Bearpark, J. J. Heyd, E. N. Brothers, K. N. Kudin, V. N. Staroverov, T. A. Keith, R. Kobayashi, J. Normand, K. Raghavachari, A. P. Rendell, J. C. Burant, S. S. Iyengar, J. Tomasi, M. Cossi, J. M. Millam, M. Klene, C. Adamo, R. Cammi, J. W. Ochterski, R. L. Martin, K. Morokuma, O. Farkas, J. B. Foresman, D. J. Fox, *Gaussian 16 Revision C.01,* 2016.

42 A. D. Becke, A New Mixing of Hartree–Fock and Local Density-Functional Theories, *J. Chem. Phys.*, 1993, **98**(2), 1372–1377, DOI: 10.1063/1.464304.

43 L. A. Curtiss, M. P. McGrath, J.-P. Blaudeau, N. E. Davis, R. C. Binning and L. Radom, Extension of Gaussian-2 Theory to Molecules Containing Third-Row Atoms Ga–Kr, *J. Chem. Phys.*, 1995, **103**(14), 6104–6113, DOI: 10.1063/1.470438.

44 E. Sanville, S. D. Kenny, R. Smith and G. Henkelman, Improved Grid-Based Algorithm for Bader Charge Allocation, *J. Comput. Chem.*, 2007, **28**(5), 899–908, DOI: 10.1002/jcc.20575.

45 M. Yu and D. R. Trinkle, Accurate and Efficient Algorithm for Bader Charge Integration, *J. Chem. Phys.*, 2011, **134**(6), 064111, DOI: 10.1063/1.3553716.

46 G. Henkelman, A. Arnaldsson and H. Jónsson, A Fast and Robust Algorithm for Bader Decomposition of Charge Density, *Comput. Mater. Sci.*, 2006, **36**(3), 354–360, DOI: 10.1016/j.commatsci.2005.04.010.

47 W. Tang, E. Sanville and G. Henkelman, A Grid-Based Bader Analysis Algorithm without Lattice Bias, *J. Phys.: Condens. Matter*, 2009, **21**(8), 084204, DOI: 10.1088/0953-8984/21/8/084204.

48 R. Dronskowski and P. E. Bloechl, Crystal Orbital Hamilton Populations (COHP): Energy-Resolved Visualization of Chemical Bonding in Solids Based on Density-Functional

Open Access Article. Published on 09 October 2025. Downloaded on 10/29/2025 11:21:30 PM.
This article is licensed under a Creative Commons Attribution-NonCommercial 3.0 Unported Licence.

Calculations, *J. Phys. Chem.*, 1993, **97**(33), 8617–8624, DOI: 10.1021/j100135a014.

49 S. Maintz, V. L. Deringer, A. L. Tchougréeff and R. Dronskowski, LOBSTER: A Tool to Extract Chemical Bonding from Plane-Wave Based DFT, *J. Comput. Chem.*, 2016, **37**(11), 1030–1035, DOI: 10.1002/jcc.24300.

50 C.-G. Zhan, J. A. Nichols and D. A. Dixon, Ionization Potential, Electron Affinity, Electronegativity, Hardness, and Electron Excitation Energy: Molecular Properties from Density Functional Theory Orbital Energies, *J. Phys. Chem. A*, 2003, **107**(20), 4184–4195, DOI: 10.1021/jp0225774.